

Short Communication

Rationally Designed Hierarchical ZnO/NiCo-LDH Hybrids for High-Performance Supercapacitors Electrodes

Sijia Jin¹, Yihui Sun², Minxuan Xu¹, Yueqin Shi¹, Fantao Meng², Xin Zheng^{1,3,*}

¹ Center for Advanced Optoelectronic Materials, College of Materials and Environmental Engineering, Hangzhou Dianzi University, Hangzhou 310018, P. R. China

² Zhejiang Hikstor Technology Co. Ltd, Hangzhou 311300, PR China

³ College of Chemistry and Materials Engineering, Zhejiang A&F University, Hangzhou 311300, PR China

*E-mail: vencen@hdu.edu.cn

Received: 3 May 2022 / Accepted: 21 June 2022 / Published: 7 August 2022

Developing a reasonable conductive structure is an effective way to construct supercapacitor electrode materials with high properties. Inspired by the way branches and stems accumulate and transfer nutrients, we fabricated hierarchical dendritic electrodes through a facile hydrothermal process to make high-capacity supercapacitors. Specifically, a self-supporting hierarchical ZnO/NiCo-LDH structure was created on carbon cloth substrates via simple processes. The hierarchical dendritic structure facilitated efficient charge transfer and active site exposure as well as the synergetic effect of providing the stacking of layered LDH nanosheets. This hierarchical ZnO/NiCo-LDH electrode possessed excellent capacitance ($22808.9 \text{ mF}\cdot\text{cm}^{-2}$ at $2 \text{ mA}\cdot\text{cm}^{-2}$) and good retention rate (85.7 % capacity retention at $15 \text{ mA}\cdot\text{cm}^{-2}$), while the capacitance of CC@NiCo-LDH was only $1620.9 \text{ mF}\cdot\text{cm}^{-2}$. This structure design provides a good prospect for high-efficiency electrochemical supercapacitors.

Keywords: Hierarchical ZnO structure; Electrode materials; Pseudocapacitors; Electrochemical performance

1. INTRODUCTION

The massive consumption of fossil energy has generated a series of problems, including environmental pollution, global warming, limited economic development, and significant damage to human beings [1-3]. In order to take more advantage of renewable energy sources such as solar, wind, and tidal energy, advanced energy storage systems (ESS) are urgently needed to solve the problem of large fluctuations in clean energy resources 4. Compared to rechargeable batteries, supercapacitors have drawn much attention because of their instantaneous high-power density, long lifetime, superior stability, and environmental friendliness 5. Commercialized supercapacitors are mostly made of carbon-

based electrode materials, which are limited in capacity due to their double-layer electrical capacitance behavior 46. Recently, pseudocapacitive materials, such as transition metal oxides and hydroxides, which exhibit much higher energy densities than electrical double-layer materials, have been extensively studied 7. Particularly, considerable scientific research efforts have been focused on layered double hydroxide (LDH) due to its unique layered structure, high theoretical specific capacitance, high redox activity, and flexible ion exchangeability 8. Among the transition metal elements, Ni and Co have been intensively studied due to their multiple oxidation states and synergistic effects 9. However, the intrinsic drawbacks of easy stacking as well as the low electronic/ionic conductivity hinder its development to some extent [10-11].

Self-supporting conductive scaffolds can effectively reduce stacking and facilitate electron-ion transport. Consequently, they have been the subject of numerous studies [12-13]. For instance, Wang et al. 14 constructed three-dimensional structured NiCo_2S_4 @NiCo nanotube arrays on Au-metalized cotton threads. The NiCo_2S_4 nanotubes act as a conductive scaffold for the Ni-Co LDH and as additional active material for capacitance. Zhao et al. 15 reported a hybrid structure consisting of NiMn-LDH grafted onto the CNT backbone, which exhibits an electrical capacitance of 2960 F g^{-1} at 1.5 A g^{-1} . Wang et al. 16 synthesized Ni-Al LDHs on exfoliated MXene sheets (MXene/LDH). Owing to the novel e-MXene substrate, the optimized MXene/LDH displays a specific capacitance value of 1061 F g^{-1} at a current density of 1 A g^{-1} . All these studies confirm that optimizing conductive scaffolds is critical to boosting electrochemical energy storage.

Herein, a hierarchical ZnO structure was created as the free-standing conductive scaffold for NiCo-LDH by a simple two-step hydrothermal method. As a promising backbone, ZnO is generally used as a template to support active materials because of its high electron mobility, chemical stability, and structure stability [17-18]. The hierarchical structure of ZnO can open more ion transport channels and provide more active sites as pathway branches to accumulate and transfer nutrients. In addition, by forming a free-standing electrode, the electrical resistance of the binder is avoided and the electron transport to the collector is accelerated. Due to these features, the hierarchical ZnO/NiCo-LDH electrodes provide high specific capacitance ($22808.9 \text{ mF cm}^{-2}$ at 2 mA cm^{-2}) and high-rate efficiency (85.7% capacity retention at $15 \text{ mA}\cdot\text{cm}^{-2}$)

2. EXPERIMENTAL SECTION

2.1. Preparation of hierarchical ZnO nanorod on CC

A two-step synthesis was used for the growth of ZnO nanorod clusters on CC. Firstly, the carbon cloths (CC, $1.5 \text{ cm}\times 1 \text{ cm}$) were placed in acetone, ethanol and deionized water in an ultrasound bath for 10 min respectively, and then dried in a drying oven at 60°C for 1 h. Next, the CC was dipped in a mixed solution (0.15 M zinc acetate in 50 mL alcohol), followed by a drying treatment at 100°C for 10 min. This process was repeated 3-4 times. Subsequently, the processed CC was annealed at 350°C for 30 min, and the CC with ZnO seed was obtained. Then, the ZnO precursor solution was prepared with a 25:25:2 volume ratio of the 0.05 M hexamethylenetetramine (HMTA) solution, 0.05 M Zinc nitrate solution, and aqueous ammonia (containing 25% ammonia). The obtained precursor solution was transferred into a 50 mL stainless-steel autoclave with as-prepared CC vertically immersed in the above precursor solution

and kept at 95°C for 12 h. After being washed several times with deionized water, the resulting products were dried at 60°C for 1 hour. then, the ZnO nanorod arrays (CC@ZnO^①) were obtained 19. The secondary ZnO nanorods were grown on CC@ZnO^① using the same method except for being heated at 90°C for 6 h in the hydrothermal reaction, which was named CC@ZnO^②.

2.2. Preparation of core-shell ZnO/NiCo-LDH electrode

The hydrothermal method was carried out as follows. A homogeneous solution was obtained by dissolving 0.244 g Ni (NO₃)₂·6H₂O, 0.132 g CoCl₂·6H₂O, and 1.000 g CTAB into 36 mL mixed solvent (volume ratio of CH₃OH to distilled water was 5:1). After ultrasonic dispersion, several pieces of as-prepared CC@ZnO^② were vertically immersed into the above solution, which was transferred into a stainless-steel autoclave and heated at 180°C for 20 h. When the reaction finished, the obtained CC@ZnO^②@NiCo-LDH was rinsed with DI water and dried at 60°C 20. Similarly, we also synthesized CC@NiCo-LDH and CC@ZnO^①@NiCo-LDH under the same conditions for comparison. The loading of active material in CC@ZnO^①@NiCo-LDH and CC@ZnO^②@NiCo-LDH is 3 mg and 5 mg, respectively.

2.3. Characterization

The morphologies of the products were characterized using a field emission scanning electron microscope (FESEM) coupled with an energy dispersive X-ray spectroscopy (EDS) instrument. Furthermore, detailed structural information was obtained using an electron microscope with high resolution (HRTEM). X-ray diffraction (XRD) with Cu-K α radiation over the 2 θ range from 10° to 80° was operated to evaluate the crystalline structure and phase characteristics. The chemical composition and elemental valences of the prepared products were evaluated by X-ray photoelectron spectroscopy (XPS).

2.4. Electrochemical measurements

An electrochemical study was conducted at room temperature using a three-electrode configuration in KOH electrolyte, using a sample, Ag/AgCl and Pt foil as working, reference and counter electrodes, respectively. Cyclic voltammetry (CV), galvanostatic charge/discharge test (GCD) and electrochemical impedance spectrum (EIS) were performed using a CHI-660D electrochemical station. The areal specific capacitance of designed electrodes was obtained according to the following equations:

$$C_s = \frac{I\Delta t}{S\Delta U}$$

Where I (A) is the discharge current; Δt (s) is the discharge time; S (cm²) is the surface area of electrode; ΔV (V) s the potential window, respectively 21.

3. RESULTS AND DISCUSSION

The synthesis route of hierarchical ZnO/NiCo-LDH hybrids is schematically presented in **Fig. 1**. After activating the carbon cloth, a multilevel ZnO structure was developed via a two-step hydrothermal synthesis. Subsequently, the NiCo-LDH shell was coated onto the hierarchical ZnO templates, creating a core-shell electrode via a facile hydrothermal reaction. The dendritic conductive scaffold of ZnO provides more active material loading points and opens more channels for ions.

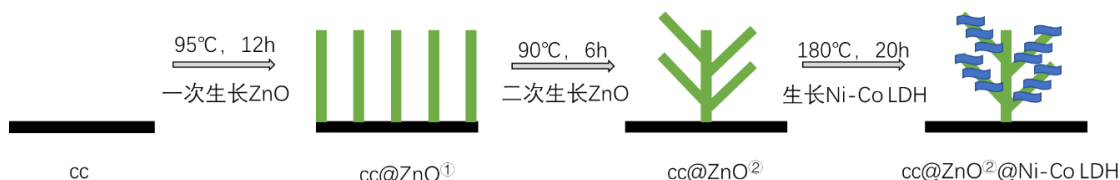


Figure 1. Schematic illustration of the fabrication process of CC@ZnO²@NiCo-LDH

Field emission scanning electron microscope (FESEM) images of different samples are shown in **Fig. 2**. As a comparison sample, NiCo-LDH was grown directly on carbon cloth, as shown in Fig. 2a. This indicates that the NiCo-LDH nanosheets with thin walls were formed uniformly on the surface of the carbon cloth which provides a considerable exposed area for the active substance. When ZnO nanorods served as the conductive support of NiCo-LDH, their morphologies were analyzed by SEM, as shown in Fig. 2(b-c). In Fig. 2b, we can see that the ZnO nanorods are all covered with active materials, and the gaps between them are completely filled with LDH, which blocks the ion intercalation channels and reduces the amount of effective active materials. As opposed to Fig. 2b, the hierarchical ZnO/NiCo LDH hybrid is visible in Fig. 2c. The special structure of ZnO nanorod clusters not only provides more growth sites for active materials and effectively inhibits the stacking of layered LDH nanosheets, but also leaves some gaps between adjacent nanorods, which promotes ion diffusion, electrolyte permeation, and structural stability 20.

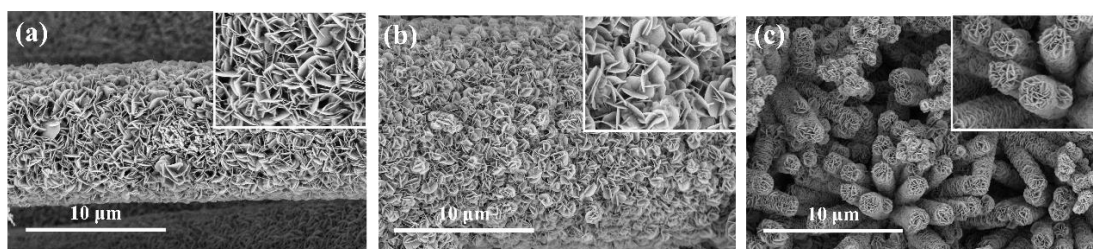


Figure 2. SEM images of (a) CC@NiCo-LDH, (b) CC@ZnO¹@NiCo-LDH, (c) CC@ZnO²@NiCo-LDH.

The XRD patterns of CC@ZnO¹ and CC@ZnO² are displayed in **Fig. 3a**. Three diffraction peaks at $2\theta = 31.8^\circ$, 34.4° , and 36.3° separately correspond to the (110), (002), and (101) planes of ZnO, which coincide with that of wurtzite-type ZnO (JCPDS No.79-0206) and illustrate that the obtained ZnO samples have high crystallinity and good orientation. In addition, a wide peak at about 26° is observed,

corresponding to the diffraction peaks of carbon derived from the carbon cloth. Fig. 3b shows the characteristic diffraction peaks of CC@NiCo-LDH, CC@ZnO^①@NiCo-LDH, and CC@ZnO^②@NiCo-LDH. The peaks at 11.6°, 23.3°, 34.3°, 35.0°, and 40.0° are consistent with the (003), (006), (101), (012), and (015) planes of a hydrotalcite-like LDH phase (JCPDS No.33-0429), implying the successful synthesis of NiCo-LDH composites. As illustrated in Fig. 3c-f, the elemental compositions and surface chemical states of CC@ZnO^②@NiCo-LDH were analyzed by X-ray photoelectron spectroscopy. Regarding the C 1s spectrum in Fig. 3c, two peaks can be seen at 284.8 and 286.5 corresponding to the aromatic-bound carbon (C=C) and carbonyl carbon (C=O), respectively. For Zn 2p XPS, two peaks appearing at 1121.3 and 1144.3 eV are ascribed to Zn 2p_{3/2} and Zn 2p_{1/2}, respectively. For the Ni 2p curve of Fig. 3e, the binding energy values of 855.0, 872.9, 861.8, and 879.2 eV correspond to Ni 2p_{3/2} and 2p_{1/2} with its satellites (indicated as “Sat.”), which correspond to the Ni²⁺ valence state, respectively. Meanwhile, two characteristic peaks at 780.8 and 796.1 eV in Fig. 3f show the spin-orbit splitting in Co 2p_{3/2} and 2p_{1/2}. This type of core-shell heterostructure contains jointed redox species of Zn, Co, and Ni, which are particularly valuable for the intrinsic faradaic activity.

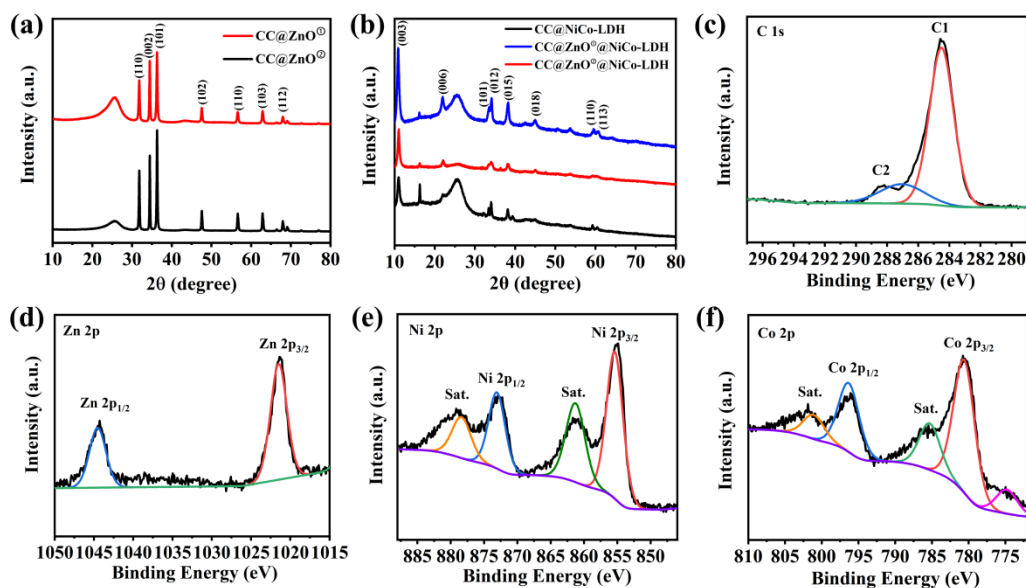


Figure 3. XRD patterns of (a) CC@ZnO^① and CC@ZnO^②, (b) CC@NiCo-LDH, CC@ZnO^①@NiCo-LDH and CC@ZnO^②@NiCo-LDH. High-resolution XPS spectra for (c) C 1s, (d) Zn 2p, (e) Ni 2p, and (f) Co 2p.

The samples were electrochemically characterized in a three-electrode configuration in 1 M KOH as the electrolyte to reveal their energy storage performance (**Fig. 4**). Fig. 4a shows the cyclic voltammetry (CV) curves of different samples at 2 mV·s⁻¹ scanning speed. The CV curve of the CC@ZnO^②@NiCo-LDH sample was found to have the largest area, indicating excellent capacity. Furthermore, GCD tests were executed at the current density of 2 mA·cm⁻² to obtain the capacitive properties of three samples (Fig. 4b). The longer discharge times and wider voltage platforms of the CC@ZnO^②@NiCo-LDH electrode indicate the high energy storage and typical pseudocapacitance characteristic, respectively, which is consistent with the CV curve.

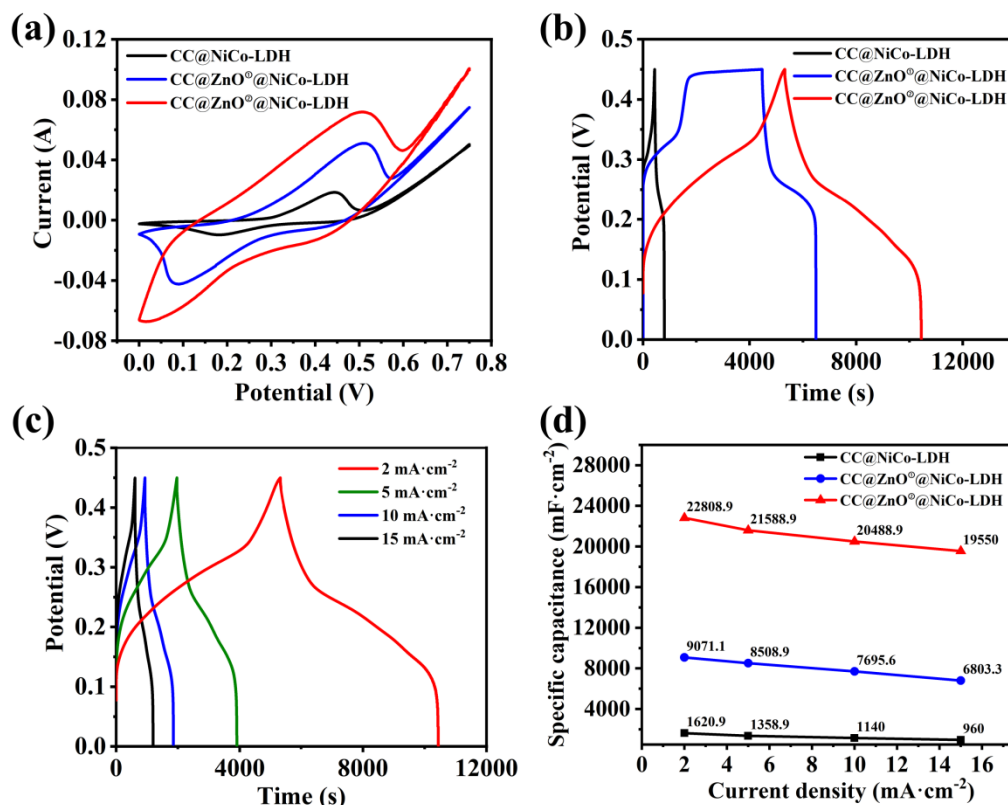


Figure 4. (a) CV curves of CC@NiCo-LDH, CC@ZnO^①@NiCo-LDH and CC@ZnO^②@NiCo-LDH at 2 mV·s⁻¹, (b) GCD curves of CC@NiCo-LDH, CC@ZnO^①@NiCo-LDH and CC@ZnO^②@NiCo-LDH at 2 mA·cm⁻², (c) GCD curves of CC@ZnO^②@NiCo-LDH at different current densities of 2 to 15 mA cm⁻², (d) capacitance of three electrodes at different current density.

The specific capacitance of CC@ZnO^②@NiCo-LDH, CC@ZnO^①@NiCo-LDH, and CC@NiCo-LDH electrodes at the current density of 2 mA·cm⁻² was calculated to be 22808.9, 9071.1, and 1620.9 mF·cm⁻², respectively. To further investigate the electrochemical properties, the GCD profiles of CC@ZnO^②@NiCo-LDH at variational current densities from 2 to 15 mA·cm⁻² are shown in Fig. 4c. As the current density increases, the quasi-symmetry of the charge and discharge curves demonstrated the remarkable reversibility and high coulombic efficiency of CC@ZnO^②@NiCo-LDH. A calculated areal-specific capacitance of the three samples at various current densities is plotted as line diagrams in Fig. 4d. The areal-specific capacitance values of the CC@ZnO^②@NiCo-LDH electrode were 22808.9, 21588.9, 20488.9, and 19550.0 mF·cm⁻², corresponding to the current densities of 2, 5, 10 and 15 mA·cm⁻² respectively, which was almost 2.5 times higher than CC@ZnO^①@NiCo-LDH and 15 times higher than CC@NiCo-LDH. It is worth mentioning that with the increasing current density, the areal-specific capacitance does not decrease significantly (85.7% capacitance retention at 15 mA·cm⁻²), better than CC@ZnO^①@NiCo-LDH (75.0% capacitance retention at 15 mA·cm⁻²) and CC@NiCo-LDH (59.2% capacitance retention at 15 mA·cm⁻²), indicating the excellent rate capability of CC@ZnO^②@NiCo-LDH.

Table 1. Comparison of the electrochemical properties of the CC@ZnO₂@NiCo-LDH electrode material and some relevant materials reported previously.

Electrode	Capacitance	Rate capability	Ref.
CoS _x @NiCo-LDH	680.8 C g ⁻¹ at 1 A g ⁻¹	76% (from 1 A g ⁻¹ to 10 A g ⁻¹)	23
NiCo-LDH/Ag/NF	2920.6 F g ⁻¹ at 5 A g ⁻¹	65% (from 5 A g ⁻¹ to 15 A g ⁻¹)	24
NiCo ₂ O ₄ @NiCo-LDHs	5810 mF cm ⁻² at 1 mA cm ⁻²	75.5% (from 1 mA cm ⁻² to 10 mA cm ⁻²)	25
NiCo-LDH/Mn ₃ O ₄	1.86 C cm ⁻² (1034.33 C g ⁻¹) at 1 mA cm ⁻²	76.88% (from 1 mA cm ⁻² to 20 mA cm ⁻²)	26
HCNs@NiCo-LDH	2558 F g ⁻¹ at 1 A g ⁻¹	74.9% (from 1 A g ⁻¹ to 20 A g ⁻¹)	26
NiCo-LDH/ZnO nanowires	1927 F g ⁻¹ at 2 A g ⁻¹	81% (from 2 A g ⁻¹ to 30 A g ⁻¹)	28
CC@ZnO ² @NiCo-LDH	22808.9 mF·cm ⁻² (4561.78 F g ⁻¹) at 2 mA·cm ⁻²	85.7% (from 2 mA·cm ⁻² to 15 mA·cm ⁻²)	This work

The specific capacity performance results of relevant electrode materials reported in recent years are listed in Table 1. The specific capacitance of our electrode (4561.78 F g⁻¹ at 2 mA cm⁻²) exceeds that of other NiCo-LDH electrodes, such as CoS_x@NiCo-LDH (680.8 C g⁻¹ at 1 A g⁻¹), NiCo-LDH/Ag/NF (2920.6 F g⁻¹ at 5 A g⁻¹), NiCo₂O₄@NiCo-LDHs (5810 mF cm⁻² at 1 mA cm⁻²), NiCo-LDH/Mn₃O₄ (1.86 C cm⁻² at 1 mA cm⁻²), and HCNs@NiCo-LDH (2558 F g⁻¹ at 1 A g⁻¹), due to the hierarchical structure of ZnO that offers enhanced conductivity and stability. Compared to ZnO-based electrodes, such as NiCo-LDH/ZnO nanowires (1927 F g⁻¹ at 2 A g⁻¹), the electrodes we fabricated have significantly improved electrochemical performance. This can be attributed to the multiple electroactive sites offered by NiCo-LDH, which exhibits multiple oxidization states. Besides, the cluster structure of ZnO nanorods opens the ions embedding channel and accelerates the exchange efficiency of electrons or ions at the electrode-electrolyte interface. In terms of capacitance, the electrodes we prepared are better than most of the reported ZnO-based and NiCo-LDH-based electrodes, indicating that hierarchical ZnO/NiCo-LDH electrodes are promising electrodes for high efficiency supercapacitors.

4. CONCLUSION

In this paper, a well-ordered ZnO structure was synthesized on carbon cloth substrates as a conductive framework. A core-shell structure was then constructed on the ZnO surface with NiCo-LDH nanosheets in situ. The CC@ZnO²@NiCo-LDH electrode exhibited a specific capacitance of 22808.9 mF·cm⁻² at 2 mA·cm⁻² and a capacitance retention rate of 85.7% at 15 mA·cm⁻². Compared to the CC@NiCo-LDH electrodes without hierarchical structure, the capacitance was enhanced by 1308%. The significant improvement in electrochemistry is due to the hierarchical structure with a massive number of active sites and fast ion diffusion. Consequently, our work provides a viable approach to constructing free-standing hierarchical electrodes and opens the possibility of adopting them in high-performance supercapacitors.

ACKNOWLEDGEMENTS

This work was supported by National Nature Science Foundation of China (No. 52102230, 11847076, 52002101, 51872069), the Zhejiang Provincial Natural Science Foundation of China (No. LQ19E020005, LQ20E020007, LQ20E020006) and Scientific Research Project of Zhejiang Education Department (Grant No. Y201942097), Starting Foundation of Hangzhou Dianzi University (No. KYS205618042).

References

1. A. González, E. Goikolea, J.A. Barrena and R. Mysyk. *Renew. Sust. Energ. Rev.*, 58 (2016) 1189.
2. D.G. Wang, Z.B. Liang, S. Gao, C. Qu and R.Q. Zou. *Coord. Chem. Rev.*, 404 (2020) 213093.
3. Poonam, K. Sharma, A. Arora and S.K. Tripathi. *J. Energy Storage*, 21 (2019) 801.
4. B. Xu, H.B. Zhang, H. Mei and D.F. Sun. *Coord. Chem. Rev.*, 420 (2020) 213438.
5. X. Zheng, K. Zhang, Y.H. Sun, S.J. Jin, Y. Li, H. Yu, H.Y. Qin and Y.Y. Ding. *J. Alloys Compd.*, 851 (2020) 156902.
6. C. Hao, L.F. Hu, M. Chen, Y. Yan and L.M. Wu. *Adv. Funct. Mater.*, 24 (2014) 934.
7. S. Najib and E. Erdem. *Nanoscale Adv.*, 1 (2019) 2817.
8. T. Wang, S.L. Zhang, X.B. Yan, M.Q. Lyu, L.Z. Wang, J. Bell and H.X. Wang. *ACS Appl. Mater. Interfaces*, 9 (2017) 15510.
9. W. Su, F. Wu, L. Fang, Jia Hu, L.L. Liu, T. Guan, X.M. Long, H.J. Luo and M. Zhou. *J. Alloys Compd.*, 799 (2019) 15.
10. H.T. Xiong, L.L. Liu, L. Fang, F. Wu, S.F. Zhang, H.J. Luo, C.Z. Tong, B.S. Hu and M. Zhou. *J. Alloys Compd.*, 857 (2021) 158275.
11. I. Shakir, M. Shahid, U. A. Rana, I.M.A. Nashef and R. Hussain. *Electrochim. Acta*, 129 (2014) 28.
12. N.T.H. Trang, H.V. Ngoc, N. Lingappan and D.J. Kang. *Nanoscale*, 6 (2014) 2434.
13. G. Meng, Q. Yang, X.C. Wu, P.B. Wan, Y.P. Li, X.D. Lei, X.M. Sun and J.F. Liu. *Nano Energy*, 30 (2016) 831.
14. Y.F. Wang, H.T. Wang, S.Y. Yang, Y. Yue and S.W. Bian. *ACS Appl. Mater. Interfaces*, 11 (2019) 30384.
15. J.W. Zhao, J.L. Chen, S.M. Xu, M.F. Shao, Q. Zhang, F. Wei, J. Ma, M. Wei, David G. Evans and X. Duan. *Adv. Funct. Mater.*, 24 (2014) 2938.
16. Y. Wang, H. Dou, J. Wang, B. Ding, Y.L. Xu, Z. Chang and X.D. Hao. *J. Power Sources*, 327 (2016) 221.
17. Y. Ouyang, X.F. Xia, H.T. Ye, L. Wang, X.Y. Jiao, W. Lei and Q.L. Hao. *ACS Appl. Mater. Interfaces*, 10 (2018) 3549.
18. C. J. Raj, M. Rajesh, R. Manikandan, J.Y. Sim, K.H. Yu, S.Y. Park, J.H. Song and B.C. Kim. *Electrochim. Acta*, 247 (2017) 949.
19. Z.M. Bai, X.Q. Yan, Y. Li, Z. Kang, S.Y. Cao and Y. Zhang. *Adv. Energy Mater.*, 6 (2016) 1501459.
20. X.J. Liu, H. Liu and X.Z. Sun. *CrystEngComm*, 22 (2020) 1593.
21. X. Zheng, Y.H. Sun, S.J. Jin, K. Zhang, Y. Li, J.L. Yan, H.Y. Qin and H.L. Ni. *Int. J. Electrochem. Sci.*, 15 (2020) 6249.
22. F. Yang, K. Zhang, W.Y. Li and K.B. Xu. *J. Colloid Interface Sci.*, 556 (2019) 386.
23. X. Liu, L. Ye, Y.Q. Du and L.J. Zhao. *Mater. Lett.*, 258 (2019) 126812.
24. T. Guan, L. Fang, L.L. Liu, F. Wu, Y. Lu, H.J. Luo, J. Hu, B.S. Hu and M. Zhou. *J. Alloys Compd.*, 799 (2019) 521.
25. S.X. Wang, Y.J. Zou, F. Xu, C.L. Xiang, H.L. Peng, J. Zhang and L.X. Sun. *J. Energy Storage*, 41 (2021) 102862.
26. N. Zhao, H.Q. Fan, M.C. Zhang, C. Wang, X.H. Ren, H.J. Peng, H. Li, X.B. Jiang and X.Q. Cao. *J. Alloys Compd.*, 796 (2019) 111.
27. J. Xu, C.J. Ma, J.Y. Cao and Z.D. Chen. *Dalton Trans.*, 46 (2017) 3276.

28. I. Shakir, M. Shahid, U.A. Rana, I.M. Al Nashef, R. Hussain, *Electrochim. Acta*, 129 (2014) 28.

© 2022 The Authors. Published by ESG (www.electrochemsci.org). This article is an open access article distributed under the terms and conditions of the Creative Commons Attribution license (<http://creativecommons.org/licenses/by/4.0/>).